

**Yuba River
New Bullards Bar to Colgate Powerhouse**

2014 Topographic Mapping Report



Prepared for: Yuba County Water Agency

By

Jason Wiener and Greg Pasternack, PhD.

University of California, Davis

July 12, 2016

Executive Summary

Topographic mapping provides the foundation for river management and science. This is the first time that a detailed topographic map has been produced of the Yuba River between New Bullards Bar Dam and Colgate Powerhouse. Airborne LiDAR data consisting of near infrared laser scans for mapping the bare Earth surface in sub-aerial terrain and green laser scans for mapping sub-aqueous bathymetry were collected by Quantum Spatial on September 27-29, 2014 during a period of low flow. Supplemental single-beam echosounder data with positioning by RTK GPS was collected subsequently within the study reach at the upstream-most deep pool and the downstream-most pools. Quantum Spatial provided initial point classification for the LiDAR data, however significant areas of boulders and exposed bedrock features were filtered out of the ground/bathymetry class using these standard procedures. As a result, a new filtering procedure was developed and implemented increasing the overall average point density from 0.35 to 1.29 pts/ft². The final map included 69,784,144 LiDAR topographic points in all.

Limitation of green LiDAR penetration to ~ 9-15 ft deep required the estimate of bathymetry of deeper locations in inaccessible areas using a calibrated function between observed water depth and color in airborne imagery at 137,022 points. This technique is usually applied in much shallower water conditions, and given the high depths present within the study reach the results were more uncertain. Best estimates were obtained for a total of 168,965 additional ground points covering an area of ~3.9 acres. For the deepest, remote pools for which there was no method available, pools were assigned bathymetry through the addition of strategically placed “augmented points” located on the basis of interpreting all available data sources. This added another 828 points. Thorough verification and merging of each individual dataset an extremely detailed and accurate topographic map and digital elevation model of the project area was created.

Cite as: Wiener, J., Pasternack, G.B. 2016. 2014 Topographic Mapping Report- Yuba River from New Bullards Bar to Colgate Powerhouse. Prepared for Yuba County Water Agency. University of California, Davis, CA.

Table of Contents

1. Introduction	1
2. Study Area	1
2.1. Segment Characteristics	5
3. Data Collection	6
3.1. Airborne Bathymetric LiDAR Data	6
3.1.1. Water Surface Elevation Filtering	10
3.2. Single Beam Sonar Data	11
4. LiDAR Re-filtering	14
4.1. Image Classification	15
4.2. LiDAR Re-filtering	17
4.2.1. Re-Filtering Results	18
5. Supplemental Data	19
5.1. Imagery Derived Depth Data	20
5.2. Augmented Points	23
6. Conclusion	23
7. References	25

Figures

Figure 1. Yuba River watershed map.	2
Figure 2. Regional vicinity map.	3
Figure 3. Closer study area map.	4
Figure 4. Cross-section showing Quantum Spatial's LiDAR point classifications.	7
Figure 5. Example of in-water LiDAR data gaps.	9
Figure 6. SB soundings data points.	13
Figure 7. Example of the Type I error regions in original LiDAR data.	16
Figure 8. LiDAR re-filtering conceptual model.	17
Figure 9. Oblique view example of pre (A) and post (B) LiDAR re-filtering.	19
Figure 10. Blue/red depth-to-X scatterplot for all LiDAR training data.	21
Figure 11. Example of imagery derived bathymetric data.	22

Tables

Table 1. Data sources for 2014 NBB-CP.	6
Table 2. First return point densities.	8
Table 3. Ground classified point densities.	8
Table 4. Summary of absolute accuracy statistics.	10
Table 5. Summary of relative accuracy statistics.	10
Table 6. Accuracy assessment of SB soundings.	11
Table 7. LiDAR vs. SB sonar data comparison summary.	12
Table 8. Pre vs. post re-filtering data summary.	18
Table 9. Original vs. final topographic data summary.	24

1. Introduction

A topographic map is a “field” that depicts a continuous representation of the land surface. Measurements identify elevations in reference to a specified datum. Despite the fact that field data is often visualized in a continuous form, topography included, all field data originates as a collection of control points that represent the surface at discrete locations. The continuity we observe is achieved through interpolation of these control points. All field data are therefore influenced by error due to the density of the control point data (i.e., interpolation error) and the accuracy of the equipment used to obtain the data (i.e., instrument error).

Topography is one of the most fundamental variables controlling ecosystem processes within a watershed, as such, it is essential to develop a good topographic map to aid in landscape decision making. In the case of rivers, topographic maps allow us to analyze the speed and direction of water flow, the capacity for geomorphic change, and the potential instream habitat conditions. Both habitat conditions and channel dynamics are important considerations in river management, particularly in regulated rivers that are actively managed to balance multiple needs and interests. High quality topographic maps are also required for river projects that will actively change landforms, such as restoration, rehabilitation, and enhancement.

The purpose of this report is to summarize the mapping effort performed in support of the ongoing Geomorphology and Physical Fish Habitats of the Yuba River between New Bullards Bar Dam and Colgate Powerhouse Project (project). Topographic data was collected in late summer 2014 along a section of the Yuba River (see Section 2 for discussion of the study area) during an extended drought when conditions were highly favorable to data collection. This mapping will facilitate a range of studies including 2-dimensional (2D) hydrodynamic modelling and habitat suitability analyses. Furthermore, the mapping will support the overall project goal to use near-census methods (Pasternack 2011) to reveal the geomorphology and physical fish habitats of the Yuba River between New Bullards Bar Dam and Colgate Powerhouse in support of managing flows and landscapes for this river corridor as well as to evaluate the potential for river rehabilitation and enhancement actions in a systematic framework. The following report outlines data collection, processing, and steps taken to assure the quality of the final mapping product(s) (2014 NBB-CP topographic map).

2. Study Area

The Yuba River is a tributary of the Feather River in north-central California that drains 3480 km² of the western Sierra Nevada range (Fig. 2). Through the 20th century the Yuba River watershed was developed and altered for multiple societal purposes typical of mountains in developed nations around the world. The watershed has an earlier history of hydraulic gold mining that is the source of much of the present alluvium in the river network (Gilbert, 1917; James, 2005). Englebright Dam was built in 1940 to trap nearly all sediment and thereby promote downstream geomorphic recovery, which continues to proceed more than 70 years later (Carley et al., 2012). As a result, the dam is a key boundary between the watershed above and the valley below. The watershed upstream of Englebright Dam has three major subbasins: the North Yuba (1,271 km²), Middle Yuba (544 km²), and South Yuba (912 km²). New Bullards Bar Dam (NBB) is a concrete arch dam on the North Yuba River near Dobbins, CA that was constructed in 1969 and is operated by Yuba County Water Agency (YCWA) for water supply and hydroelectric power generation. Upstream of this reservoir the North Yuba catchment lacks any

major impoundment. Like Englebright Dam, New Bullards Bar Dam is a complete barrier to bedload transport and has a very high trapping efficiency for suspended sediment, except for some fine-grained wash load. It also catches and traps all large wood, except for a small amount that might pass over the emergency spillway if it gets past a protective boom barrier at the spillway entrance. Thus, it too functions as a key demarcation in the watershed. Meanwhile, many small impoundments and infrastructure facilities on the Middle and South Yuba Rivers exist much higher up in the stream network originally built to support hydraulic mining but now repurposed for hydroelectric power generation, local water supply, and inter-basin export to the Bear and American Rivers (Snyder et al., 2004; YCWA, 2012).

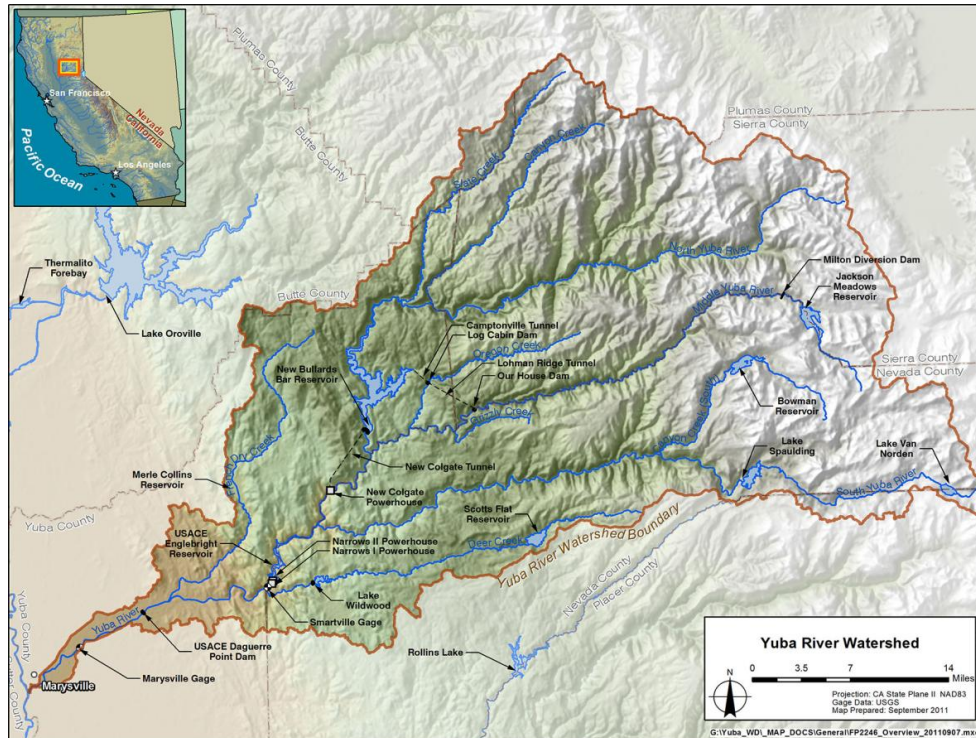


Figure 1. Yuba River watershed map.

The study area includes ~ 380 acres of the North (N.) Yuba River below New Bullards Bar Dam and the portion of the Yuba River from the confluence of the N. Yuba River and Middle Yuba River to just upstream of Colgate Powerhouse (Fig. 2 and Fig. 3). Within the entirety of the study area the river corridor is confined in a steep-walled bedrock canyon. The present condition of the N. Yuba/Yuba River within the study area is a heavily regulated system used for flood protection, power generation, water supply, and environmental management.

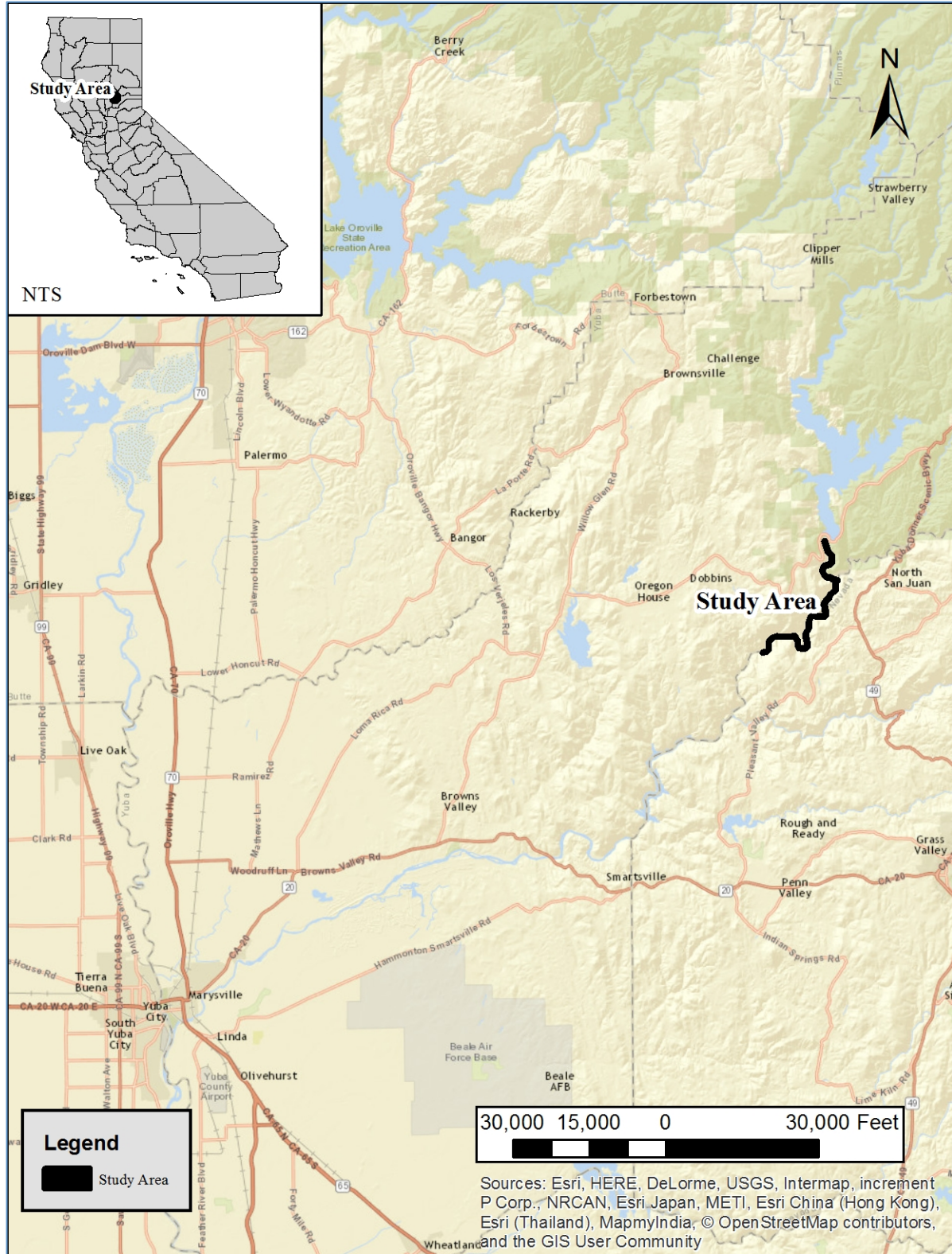


Figure 2. Regional vicinity map.

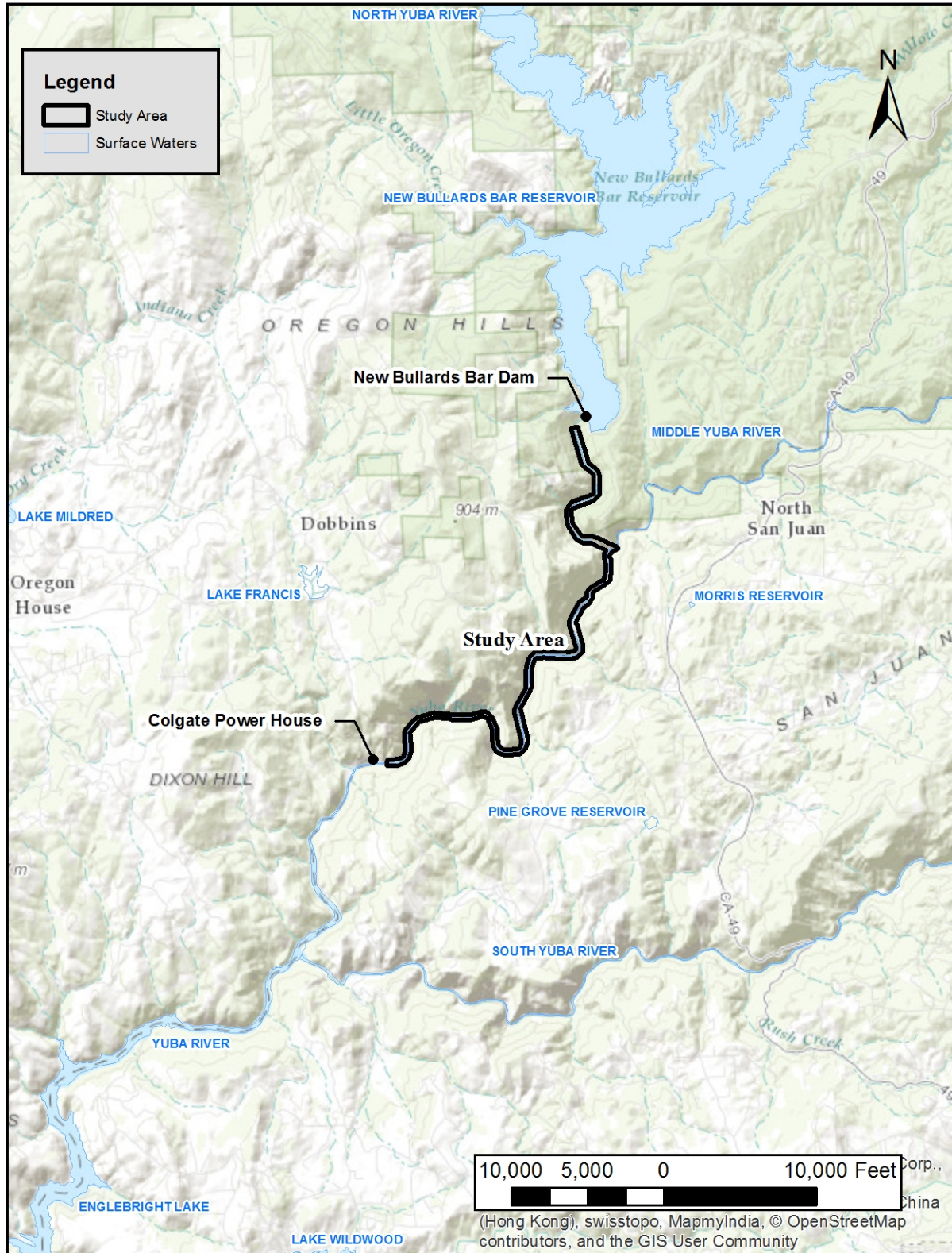


Figure 3. Closer study area map.

2.1. *Segment Characteristics*

YCWA operates New Bullards Bar Dam by capturing winter and spring runoff from rain and snowmelt. Consequently, NBB normally reaches its annual peak storage at the end of the spring runoff season and then is gradually drawn down until its lowest elevation is reached in mid-winter. The reservoir does not undergo substantial daily changes in elevation due to operations of YCWA facilities (YCWA, 2011). The portion of the N. Yuba River below New Bullards Bar Dam above the confluence of the Middle Yuba River receives minimal releases from New Bullards Bar Dam in accordance with the Federal Energy Regulatory Commission (FERC) minimum operational flow requirement of 5 cubic feet per second (cfs). Additional sources of water in the reach are seepage from the dam, other operational releases, flow over the emergency spillway, and accretionary flows.

New Colgate Powerhouse is located on the north side of the Yuba River ~ 8.1 miles downstream of New Bullards Bar Dam and ~ 1.7 miles upstream of the normal maximum water surface elevation of Englebright Dam. The powerhouse receives water from New Bullards Bar Dam via the 5.2-mile-long New Colgate Power Tunnel and Penstock and can produce an outflow of ~ 3,400 cfs. The powerhouse operates as a peaking facility, which means it can ramp up from a minimum flow of a few cfs to its maximum flow in just 10 minutes, and does so frequently, so the hydraulics in this reach are disconnected from the upstream reaches (YCWA, 2011).

The Middle Yuba River has a complex system of dams and diversion for water resources management. Extending eastward into the Sierra with the headwater near Jackson Meadows, Middle Yuba flows are captured in Jackson Meadows and Milton Reservoirs. Water from Milton Reservoir (Milton Diversion Dam) is diverted via the Yuba-Bear Project's Milton-Bowman Tunnel to Bowman Lake (South Yuba Basin). The Yuba-Bear Project has minimum instream flow requirements below the Milton Diversion Dam. Downstream of Milton Reservoir the Middle Yuba is confined within steep narrow canyons until Our House Dam. Our House Dam, ~ 13 miles upstream of the confluence with the N. Yuba is used to retain and transport water to New Bullards Bar Dam. Water is conveyed from the Middle Yuba to the adjacent Oregon Creek via the Lohman Ridge Tunnel where it is subsequently conveyed to New Bullards Bar Dam via the Camptonville Tunnel. Middle Yuba flows below Our House Dam to the confluence of Oregon Creek consist of releases from Our House Dam (note FERC minimum operational flow requirement of 30 cfs from June 16 – April 14 and 50 cfs from April 15 – June 15) as well as seepage from the dam, flow over the emergency spillway (when flows exceed the Lohman Ridge Tunnel Diversion capacity of 860 cfs), and accretionary flows.

Oregon Creek connects to the Middle Yuba River ~ 4.4 miles upstream of the confluence with the N. Yuba River. Log Cabin Dam located approximately 3.8 miles upstream of the Middle Fork confluence is used to retain and transport water to New Bullards Bar Dam as previously described. Flows above Log Cabin dam are unregulated. Oregon Creek flows below Log Cabin Dam to the confluence of Oregon Creek consist of releases from Log Cabin Dam (note FERC minimum operational flow requirement of 8 cfs from June 16 – April 14 and 12 cfs from April 15 – June 15) as well as seepage from the dam, flow over the emergency spillway (when flows exceed the Camptonville Tunnel diversion capacity of 1,100 cfs), and accretionary flows.

Diversions to and from the Middle fork and Oregon Creek increase the hydrologic complexity of these features and disrupt natural flow patterns. Below the confluence of Oregon Creek and the Middle Fork of the Yuba to the confluence of the N. Yuba water consist of the previously described sources and any additional accretionary flow. Similarly, flows downstream

of the Middle fork N. Yuba confluence to the downstream study area boundary comprise these upstream flows and any accretionary flow.

Several nominal tributaries discharge to the N. Yuba/Yuba River along the study area contributing appreciable surface flow only during storm events. Channelized flow in these drainages is ephemeral. The most significant drainage is Sweetland Creek located approximately 4.3 miles upriver of Colgate powerhouse. Despite the relatively large drainage area compared to other drainages Sweetland Creek flow is still ephemeral and nearly imperceptible in summer months.

3. Data Collection

Data collected for the 2014 NBB-CP topographic map comprises airborne bathymetric LiDAR and single beam (SB) sonar. The vast majority of the data comes from the airborne bathymetric LiDAR, which uses a green laser to penetrate the water column and a near-infrared (NIR) laser that provides better delineation of terrestrial features. SB sonar data was used, where feasible, to fill in the data gaps in deep pools where the green LiDAR was not able to penetrate through to the streambed. **Table 1** outlines each survey method, location(s), and date(s) of acquisition. Each method of data collection is described in greater detail in the sections below.

Table 1. Data sources for 2014 NBB-CP.

Data	Location(s)	Dates(s)
SB Sonar	Second Pool Below New Bullards Bar Dam	7/8/2015
SB Sonar	First pool above Colgate Powerhouse	07/092015
SB Sonar	Corner pool above Colgate Powerhouse	07/092015
Airborne LiDAR	Entire Study Area	09/27-29/2014

All of the data, except for the 2014 LiDAR, was collected in California State Plane Zone 2 NAD83 U.S. Survey Feet. In 2011 there was an update to the NAD83 datum and the 2014 LiDAR data was collected using the 2011 update, California State Plane Zone 2 NAD83 (2011) U.S. Survey Feet. All other survey data has been re-projected into this new coordinate system in ArcGIS to allow direct comparison. All vertical data is referenced to the NAVD 88 (Geoid 12A) vertical coordinate system.

3.1. Airborne Bathymetric LiDAR Data

Quantum Spatial collected combined NIR and green LiDAR data on September 27-29, 2014 during a period of low flow, approximately 31.9 cfs total gaged flows within the study area. Low flows expose more of the river corridor for the NIR laser and reduce the depth needed for the green laser to penetrate through the water column. Processing of the data by Quantum Spatial prior to delivery included:

- 1) Resolving the kinematic corrections for aircraft position data and developing a smoothed best estimate of trajectory (SBET).
- 2) Calculating the laser point positions using the SBET.

- 3) Performing a manual relative accuracy calibration using the tie-plane methodology and filtering erroneous points.
- 4) Using ground classified points to test relative accuracy (i.e. agreement between overlapping flight lines). Performing line-to-line calibrations for attitude parameters (pitch, roll, heading), mirror flex, and GPS drift.
- 5) Creating a water's edge breakline to distinguish between bathymetric returns and terrestrial returns.
- 6) Correcting for refraction through the water column for bathymetric returns.
- 7) Classifying the resulting data into ground (includes bathymetric points), water surface, water column, noise, and default (includes structures, vegetation, and noise) point classes.
- 8) Assessing the statistical absolute accuracy via direct comparisons of ground classified points to ground control survey data.
- 9) Manually reviewing and finalizing data classifications.
- 10) Generating 3.0 foot resolution bare earth and highest return rasters.
- 11) Exporting 1.5 foot NIR and green laser intensity rasters.

Figure 4 shows a representative cross-section of the LiDAR data with the point classifications used by Quantum Spatial. The water surface points come from reflectance off the water surface by the NIR laser. The ground/bathymetry points come from the green and NIR laser in the terrestrial environment and only the green laser within the wetted channel. Note the lower density of ground identified points below canopy vegetation in the left portion of the cross-section; whereas, in the right portion of the cross-section many ground returns appear to be misclassified within the default classification.

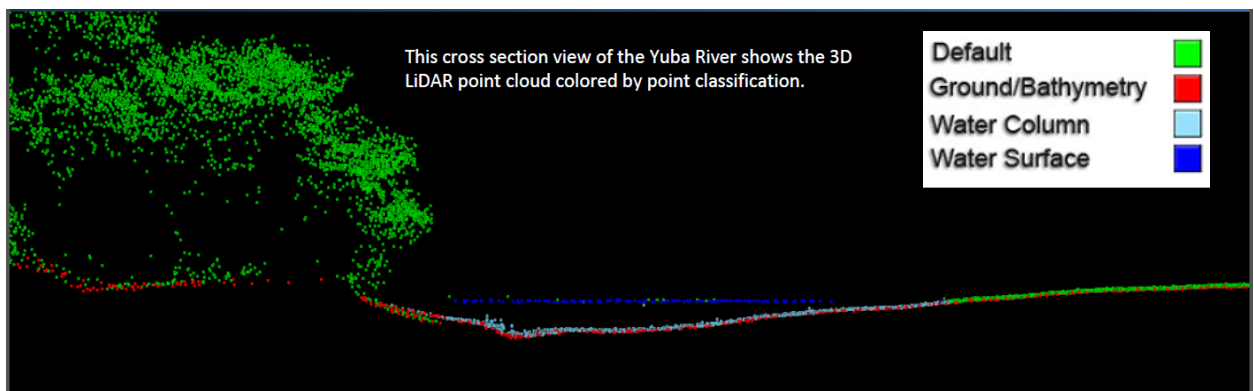


Figure 4. Cross-section showing Quantum Spatial's LiDAR point classifications.

NIR and Green LiDAR have inherent water depth penetration limitations. NIR is nearly completely absorbed by water and therefore has very poor penetration capabilities and limited capacity for use in obtaining bare-earth elevations within any open water areas greater than 1-2 feet deep and possibly not even at these depths (depending on water conditions). While green LiDAR can penetrate water, thus recording bare-earth elevations, depth penetration is still limited and the laser pulse is often fully absorbed within areas deeper than 10 feet (again this depends on water conditions and other factors). Several deep pools are present within the study area river corridor with depths preliminary estimated to exceed 20 feet. The green laser was able to penetrate water depths up to a maximum of 17.1 feet (5.2 meter) and regularly had returns in the 9-10 foot depth range (3 meters). Despite the excellent depth penetration, the survey did not

yield ground returns for numerous in-water areas located along the entirety of the river corridor (Fig. Error! Reference source not found.). This lack of returns is due to several factors including the previously mentioned deep water areas, terrain complexity limiting the ability for reception of laser pulses, canopy vegetation interference, and turbulence on the water surface.

Conservatively, the survey did not yield returns over a total area of approximately 10.1 acres within the in-water areas of the river corridor. This represents approximately 22.06% of the open water area present during the time of the survey¹. In addition to the in-water areas, significant numbers of boulder and exposed bedrock features were filtered out of the ground/bathymetry point classification provided by Quantum Spatial. Quantum Spatial revisited this issue and corrected numerous areas, but the issue was still widespread after the final data delivery (See Section 4).

Within the covered areas, LiDAR performance from the flight was exceptional. First return densities give a representation of the number of laser pulse returns per area (excluding echoes). The data shows that actual point densities far exceeded the target point densities with first return point densities for the green and NIR sensors above 1 point/ft² (Table 2)². The density of ground points classified by Quantum Spatial is presented in Table 3.

Table 2. First return point densities.

First Return Type	Target Point Density	Actual Point Density
Green Sensor	0.37 pts/ft ²	1.25 pts/ft ²
	4 pts/m ²	13.50 pts/m ²
NIR Sensor	0.74 pts/ft ²	1.14 pts/ft ²
	8 pts/m ²	12.23 pts/m ²
Combined	1.11 pts/ft ²	2.38 pts/ft ²
	12 pts/m ²	25.67 pts/m ²

Table 3. Ground classified point densities.

Ground Return Type	Average Point Density
All Ground Classified Returns	0.37 pts/ft ²
	3.96pts/m ²
Bathymetric Bottom Returns	0.21 pts/ft ²
	2.30 pts/m ²

¹ Area based on imagery classified open water area (See Section 5 for details).

² All LiDAR data metrics presented herein were documented by Quantum Spatial and include data collected within the Study Area as well as a portion of the Lower Yuba River.

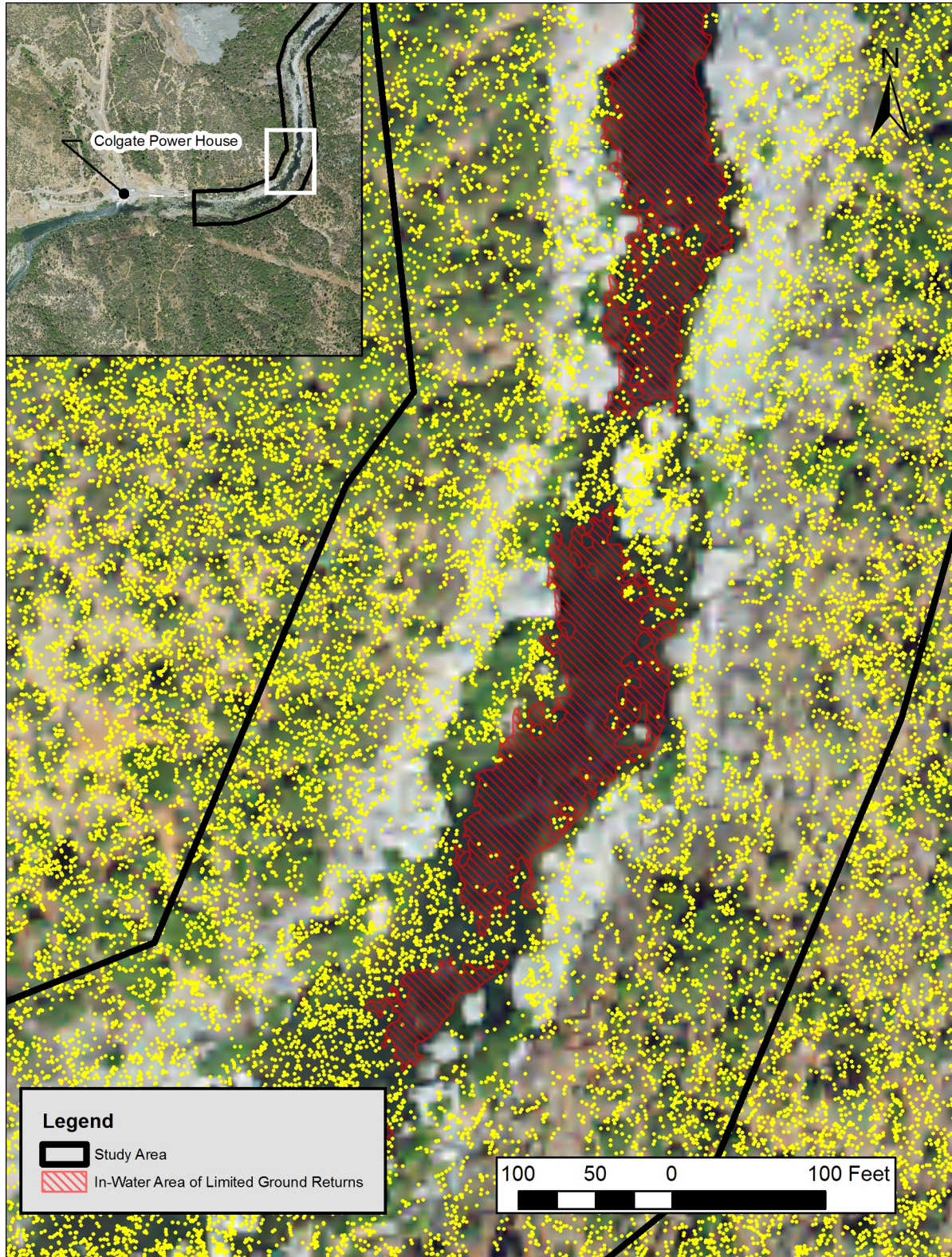


Figure 5. Example of in-water LiDAR data gaps.

Absolute accuracy is an estimate of the error of the LiDAR derived ground surface when compared to a more accurate survey method. Quantum Spatial compared the LiDAR ground surface to 23 ground check points and 24 bathymetric check points that were developed from an RTK-GPS survey. The Fundamental Vertical Accuracy (FVA) is a measure of error reported at the 95% confidence level, i.e. $1.96 \times \text{Root Mean Square Error (RMSE)}$. The FVA for ground points and bathymetric points is 0.123 ft and 0.384 ft, respectively (**Table 4**).

Table 4. Summary of absolute accuracy statistics.

	Sample	Average	Median	RMSE	Standard Deviation	FVA
Ground Check Points	23	0.025 ft	0.020 ft	0.063 ft	0.059 ft	0.123 ft
		0.008 m	0.006 m	0.019 m	0.018 m	0.038 m
Bathymetric Check Points	24	0.100 ft	0.138 ft	0.196 ft	0.172 ft	0.384 ft
		0.030 m	0.042 m	0.060 m	0.052 m	0.117 m

Relative accuracy is an estimate of the internal consistency of the LiDAR data. It is checked by comparing the identification of the same surface by overlapping flight lines. Quantum Spatial calculated the relative accuracy of the NIR and green laser using 125 and 122 surfaces, respectively. The relative accuracy reported at the 95-percentile ($1.96 \times \text{Standard Deviation}$) is 0.103 ft and 0.158 ft for the NIR and green lasers, respectively (**Table 5**).

Table 5. Summary of relative accuracy statistics.

	Sample	Average	Median	RMSE	Standard Deviation	$1.96 \times \text{SD}$
NIR Laser (terrestrial)	125 surfaces	0.098 ft	0.142 ft	0.154 ft	0.053 ft	0.103 ft
		0.030 m	0.043 m	0.047 m	0.016 m	0.032 m
Green Laser	122 surfaces	0.160 ft	0.249 ft	0.236 ft	0.081 ft	0.158 ft
		0.049 m	0.076 m	0.072 m	0.025 m	0.048 m

3.1.1. Water Surface Elevation Filtering

A water surface point dataset was provided by Quantum Spatial as part of the LiDAR delivery. The water surface of a river is generally flat (even in a high gradient confined mountain canyon), except within steep sections such as waterfalls, steps, rapids, riffles, and boulder fields. Therefore, the water surface elevations at coincident points should be within $\sim 0.5'$ of each other, especially within flat river sections. Review of the water surface LiDAR, primarily through visualization and iterative moving window selections, indicated the presence of numerous erroneous points. These errors were likely vegetation, high boulder points or water column points misidentified as the water surface. A systematic and iterative process was completed to remove spuriously high water surface points. A spatial join of the “scrubbed” water surface elevation (WSE) dataset with the LiDAR ground points allowed generation of water depths for each LiDAR ground point, as appropriate (e.g. only points resulting in positive water depths). The mean distance between nearest WSE and ground point was 4.8 feet (1.5 meters), $n = 1,762,213$.

3.2. Single Beam Sonar Data

Echo-sounder surveys are an effective and common way to obtain bathymetric data and may consist of single beam (SB) or multi-beam survey equipment. SB sonar data collection was used to fill gaps in the bathymetric data where feasible. SB sonar survey methods involve sending an acoustic pulse from a sonar transducer to the bottom and measuring the time for the pulse to return. Depth is simply calculated using the speed of sound and the time of the trip ($\text{depth} = (\text{time} \times \text{speed of sound}) / 2$), dividing by 2 accounts for the total trip length. Accurate measurement requires accurate location of the transducer for each measurement, obtained using a precision GPS unit. Error in measurement results from intrinsic error in the time and speed measurements, uncertainty in the speed of sound within water which is influenced by temperature, salinity, and pressure, and error in GPS positional accuracy.

Single beam echo sounding data was collected by kayak between July 8 and 9th 2015 at three locations within the study area. The survey included two pool locations upstream of Colgate Powerhouse (CP Lower Pool and CP Corner Pool) and the very deep pool downstream of New Bullards Bar Dam (NBB Second Pool) to which the dam's emergency spillway discharges (Fig. 6). Surveyable areas were severely limited by access constraints and rugged terrain within the river canyon. The SB sonar data was collected using an Ohmex Sonarmite and its 3D position was tracked using a Trimble 5800 Real Time Kinematic (RTK) GPS tied to a local base station on one of two benchmarks established through static surveys conducted at the same time as bathymetric data was collected. Soundings data were recorded on the TSC3 data collector for the GPS and integrated with positional data. These data were then post processed within Trimble Business Center. After waiting the necessary time for a precise solution, NOAA's Online Positioning User Service (OPUS) was used to obtain the coordinates of static survey positions. Then all point positions were adjusted to the correct benchmark coordinates following a standard workflow provided by California Surveying and Drafting in Sacramento, CA. The processed data was imported from the tabular XY format into a shapefile using ArcGIS and projected into the project coordinate system.

Following post-processing SB sonar data were reviewed for quality assurance and compared to the LiDAR data to determine their offsets and relative accuracy. Review of soundings involved 3D visualization to identify erroneous points and review of point accuracy information. No data points were excluded based on visualization or due to accuracy issues. Table 6 depicts the reported GPS horizontal and vertical accuracy of the soundings data by location.

Table 6. Accuracy assessment of SB soundings.

Location	Horizontal Accuracy (ft)			Vertical Accuracy (ft)			n
	Minimum	Maximum	Mean	Minimum	Maximum	Mean	
CP Corner Pool	0.032	0.679	0.0989	0.059	0.98	0.1971	5124
CP Lower Pool	0.037	0.325	0.094	0.058	0.54	0.166	662
NBB Second Pool	0.078	0.282	0.143	0.125	0.889	0.355	1599

Comparison of the LiDAR ground data to the soundings data was completed for each of the three sounding survey areas respectively. Soundings data were joined to the nearest LiDAR ground points using different sized moving windows. A balance is required in the search

window size between returning a sufficient number of points to characterize data trends while not introducing unnecessary error from large search windows and spatially distant points. A search window of 10 cm was selected to achieve this balance where smaller windows yielded too few joined points to characterize the data and trends present. The difference between LiDAR depth³ and sounding depth was computed for each point. With the exception of NBB Second Pool, sounding data more consistently under-predicted water depths (e.g. over-predicted the bed elevation) compared to the LiDAR data. Soundings data was corrected based on the mean signed difference for each area, respectively. Table 7 summarizes the comparison between the LiDAR and sounding depths.

Table 7. LiDAR vs. SB sonar data comparison summary.

Location	Mean (ft)		Standard Deviation (ft)		Max Difference (ft)		Percentage of total soundings at location		n
	Signed	Unsigned	Signed	Unsigned	Signed	Unsigned	Signed	Unsigned	
CP Corner Pool	-0.27	0.43	0.53	0.41	1.71	1.71	10.73	10.73	545
CP Lower Pool	-0.29	0.59	1.09	0.96	12.16	12.16	11.09	11.09	71
NBB Second Pool	0.17	0.32	0.38	0.25	0.68	0.68	0.69	0.69	11

³ LiDAR depth is determined based on the difference between the ground elevation and nearest water surface elevation point.

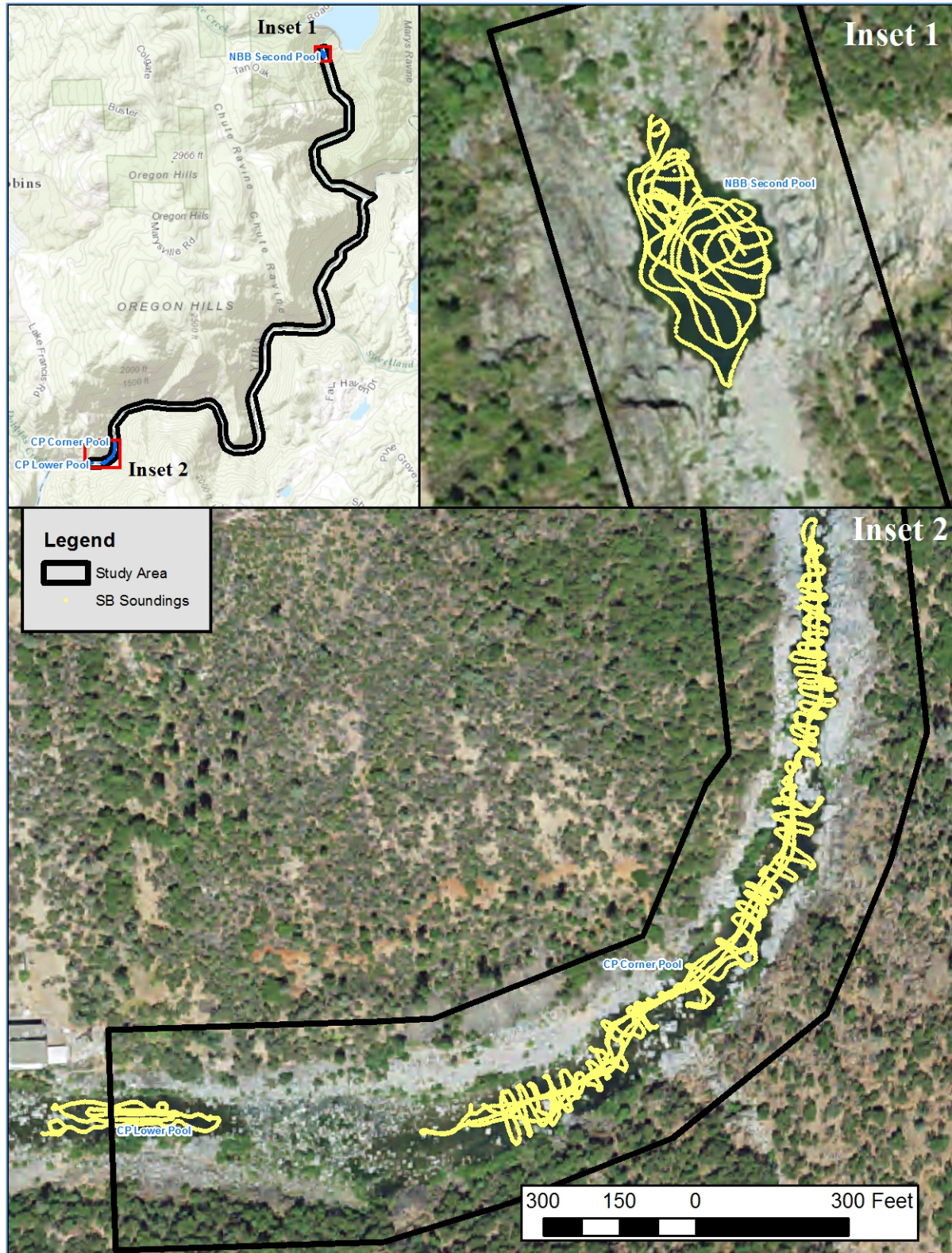


Figure 6. SB soundings data points.

4. LiDAR Re-filtering

Filtering of raw LiDAR data is standard practice in separating point cloud data into terrain (e.g. the land surface) and non-terrain (e.g. vegetation or man-made structures) features. Numerous algorithms are available that automate this process, each with unique tradeoffs in the ability to properly classify land surfaces. The most common approaches are classified into elevation difference, slope-based, morphological, and multi-scale techniques (BOR 2012). The classification tradeoff typically focuses on the type of error favored by a particular method where Type I errors reject true ground points (omission error) and Type II error incorrectly classify ground points (commission error). Factors important to the amount of total error (Type I plus Type II) include steep slopes, landscape discontinuities, bridges, complex scenes, outliers, vegetation on slopes, and low point densities (Sithole and Vosselman 2004).

Most existing algorithms focus on reducing Type II error, a point evidenced by review of the LiDAR provided for the study area (e.g. data appears to have greater Type I errors). Terrain within the study area and particularly the river corridor is highly variable containing areas of steep slopes, variable vegetation type and density, boulder fields, steep and abrupt bedrock cliffs, large areas of exposed bedrock, and complex step-pool transitions. During review of provided bare-earth LiDAR files (ground points) in comparison aerial imagery as well as the unclassified or “Default” LiDAR files, it became obvious that the filtering algorithm used significantly over-filtered and removed a substantial number of ground points associated with the many high variability terrain features in the study area. Quantum Spatial revisited this issue and corrected numerous areas, however the issue remained persistent in the final data delivery.

Figure 7 depicts an example of delineated areas potentially suffering from Type I errors. The areas shown as lacking data were systematically derived based on an inverse selection of polygons aggregated from the LiDAR ground returns with in-water areas (See Section 3.1) and areas of dense vegetation removed such that remaining areas are predominately ground features. Close observation of the figure indicates where individual large boulders were completely filtered out of the resulting ground dataset. This coarse estimation indicates a total area of 85.3 acres, ~22.45% of the study area where significant ground data may have been filtered out completely. Review of the Default dataset shows that many of these over-filtered points may exist in this classification and have the potential to be returned to the ground/bathymetry model if properly identified.

Many publically available LiDAR filtering algorithms exist for classifying ground points that implement one of several general methodologies described above. Developing an effective process to reclassify and reincorporate these Type I errors back into the ground dataset is an important step to ensure model outputs accurately calculate water depths, velocities, hydraulics, landforms and other desired outputs. The primary concern in the reclassifying process is a cost-benefit of properly classifying previous Type I errors without overclassifying new Type II errors.

Research by BOR (2012), Sithole and Vosselman (2004), and Zhang and Whitman (2005) indicate that slope-based methods tend to perform best in complex terrains and favor Type II error over Type I errors. The adaptive tin approach is one slope-based that has been shown to be particularly effective in areas of highly variable terrain (e.g. dense cities and steep wilderness environments). The LAsTools “lasground_new.exe” tool is based on the adaptive tin approach developed by Axelsson (2010), where an adaptive TIN is created with the input of some user-defined thresholds in order to separate ground points from vegetation, structures, or noise. One essential algorithm input is the “step size” which is used to designate a search

distance for identifying the next adjacent ground point to densify the TIN. For areas with high topographic variability (e.g., boulder fields and bedrock outcroppings), a small step size is needed to adequately resolve the topographic features, but as discussed this can potentially introduce errors by identifying non-ground returns as ground. For example, in vegetated areas where there are low densities of ground returns because the canopy intercepts the laser pulses, a small step size would identify near-ground vegetation returns as ground. Similarly, man-made features (e.g. houses and bridge abutments) would also be identified as ground if a sufficiently small step size is chosen.

To help address the misclassification issue image classification was completed within the study area allowing selective filtering to be implemented in areas of bare earth land cover. Additionally, several iterations using different step sizes were explored to identify the preferred settings. The steps for this process are outlined in the sections below.

4.1. Image Classification

Supervised image classification techniques (ESRI 2012) were used to classify aerial imagery into the following categories: open water, boulder/bedrock/open ground, and vegetation. The goal of this classification was to generate a boulder/ground land classification mask to be used to selectively filter the existing LiDAR data. The imagery source used in the classification was the 4-Band 2014 National Agriculture Imagery Program (NAIP) 1-meter resolution imagery. The source imagery was obtained on July 13, 2014, which provided the added benefit of being close to the date of LiDAR acquisition. The imagery was projected from its native WGS 1984 Web Mercator coordinate system into the project coordinate system such that it could be georeferenced to the LiDAR data. The LiDAR intensity data was used as the reference dataset in the georeferencing process. Classification was accomplished using the maximum likelihood classification tool and post-processed using the majority filter and boundary clean tools in ArcGIS. Additional visualization and editing of the data was completed to aggregate classes, remove small isolated polygons, and reduce unnecessary complexity for more appropriate use in processing the LiDAR data.

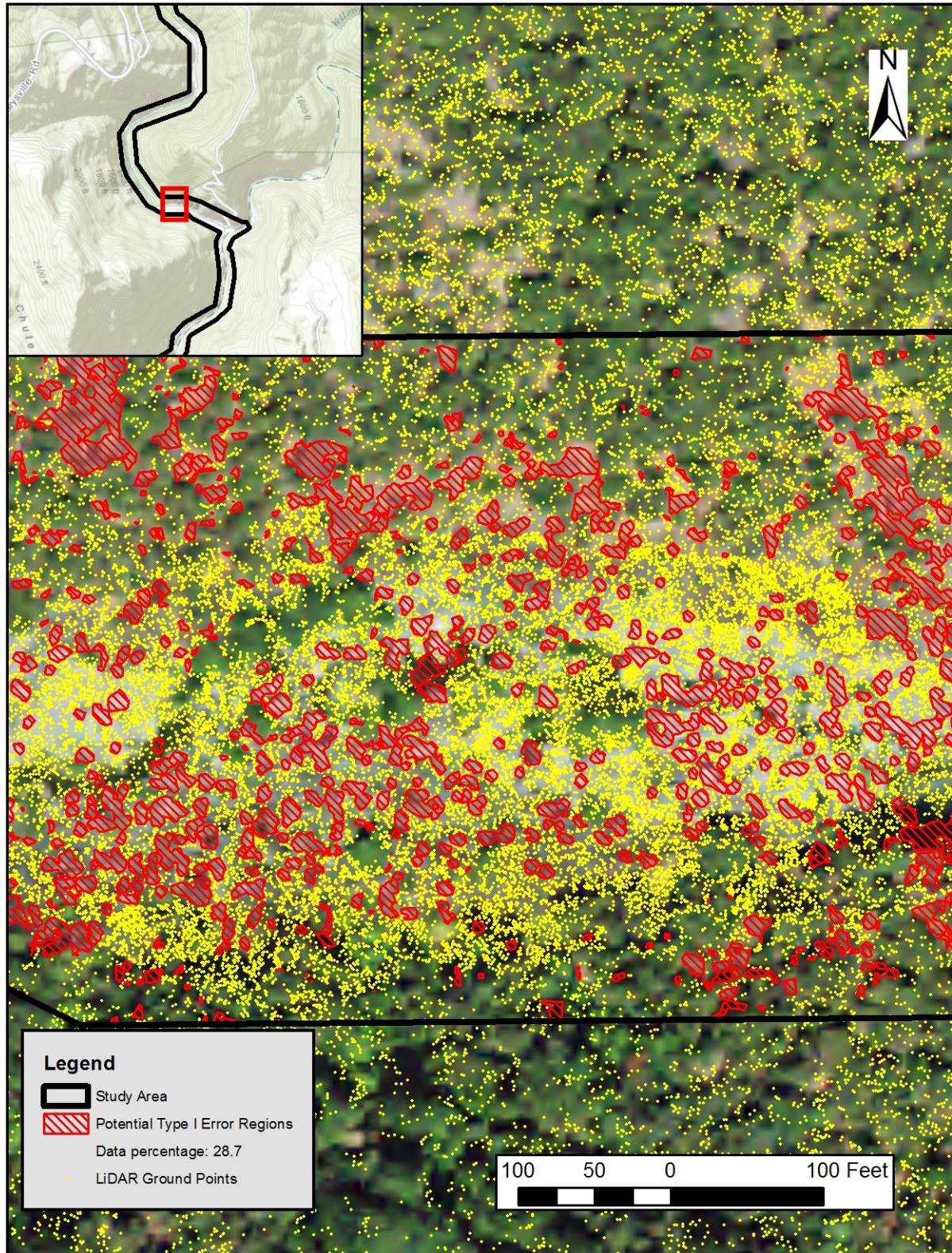


Figure 7. Example of the Type I error regions in original LiDAR data.

4.2. LiDAR Re-filtering

Figure 8 depicts the general conceptual model implemented in the LiDAR re-filtering process described step-wise below.

- The default and ground LiDAR datasets were merged and retilled with a buffer (retiling required for use of LASTools, buffer to avoid edge effect in further processing). The merging of these data is to generate high point densities and the presence of the previously identified ground points aids in the revised ground point classification.
- The merged dataset was processed twice using the lasground_new.exe tool. The first iteration implemented a small step size to retain the finer variability of the land surface. The intent of this processing was to preferentially return more ground points thus addressing the Type I errors in the original dataset and slightly favoring Type II errors. The processing settings in this iteration were named the “boulder settings”. The second iteration implemented a larger step size with the intent of mimicking the processing completed by Quantum spatial where Type II errors are avoided but potentially returning a small portion of lost ground points. The processing settings in this iteration were named the “hillside settings”.
- The boulder/bedrock/bare earth image classification file was used to clip the processed LiDAR dataset accordingly. The more aggressive “boulder setting” data was clipped to the areas within the land classification file whereas the “hillside setting” data was clipped to the inverse.
- Buffer points were removed from the resulting LiDAR datasets and the data including the original ground LiDAR data was merged. The original ground data was merged to ensure all previously identified ground points remained in the final data set.
- All duplicate points were removed and ground points were extracted into a final ground dataset.
- Lastly, a significant amount of visualization and review of the resulting dataset was completed that included hand editing and removal of erroneously classified ground points.

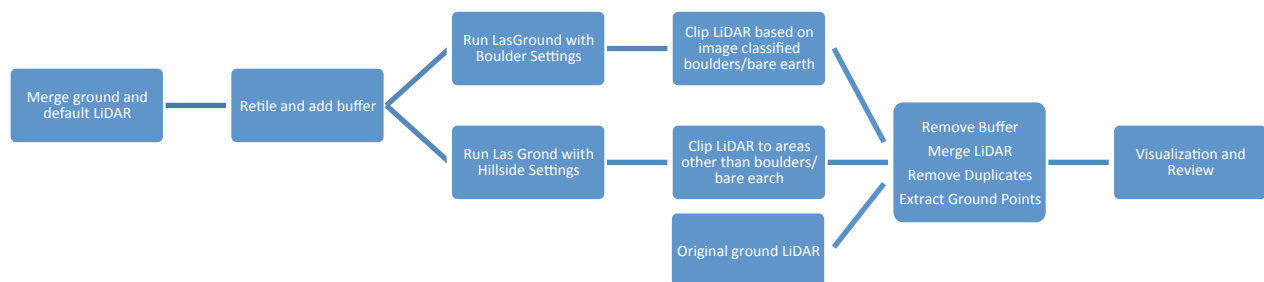


Figure 8. LiDAR re-filtering conceptual model.

A number of test iterations were completed in developing the “boulder settings” and “hillside settings”. This testing strived to strike a balance between Type I vs. Type II errors and particularly confidence in the “boulder setting”, that points added back into the ground/bathymetry classification improve the resolution of the land surface without introducing

significant errors. Iteration testing was primarily completed through visualization and comparison with aerial imagery. Review of the final dataset did indicate the presence of erroneously classified ground points. This misclassification was observed to be related to two trends in the data: 1) Areas of dense planar non-ground points and 2) The interface between steep cliff faces and the river channel. Visualization and hand editing of the final data was necessary to address these errors as described in the step-wise process above.

4.2.1. Re-Filtering Results

Error! Reference source not found. shows an example of the pre and post re-filtered land surface within a small portion of the study area. Note the substantial increase in detail added following the re-filtering process. Review of point information indicates the re-filtering process returned a substantial number of ground points reducing the average spacing between points and increasing point densities. Table 8 provides a summary of the resulting point increases between the original and re-filtered data. The summary includes information for the both entire extent of the LiDAR acquisition and specific to the study area, which was the focal point of the re-filtering process.

Table 8. Pre vs. post re-filtering data summary.

Dataset	Total Ground Points	Average Point Spacing (ft)	Average Point Density (points/ft ²)	Percent difference # of points from Quantum Spatial ¹	Percent difference point spacing from Quantum Spatial ¹	Percent difference point density from Quantum Spatial ¹
Quantum Spatial ground LiDAR	20,901,576	1.94	0.27	N/A	N/A	N/A
Re-filtered ground LiDAR	69,598,076	1.09	0.84	232.98%	-43.81%	211.11%
Quantum Spatial ground LiDAR (Study Area)	5,388,037	1.68	0.35	N/A	N/A	N/A
Re-filtered ground LiDAR (Study Area)	21,279,867	0.88	1.29	294.95%	-47.62%	268.57%

¹Percent differences are relative to the appropriate quantum spatial dataset, i.e. either the entire dataset or the study area, respectively.

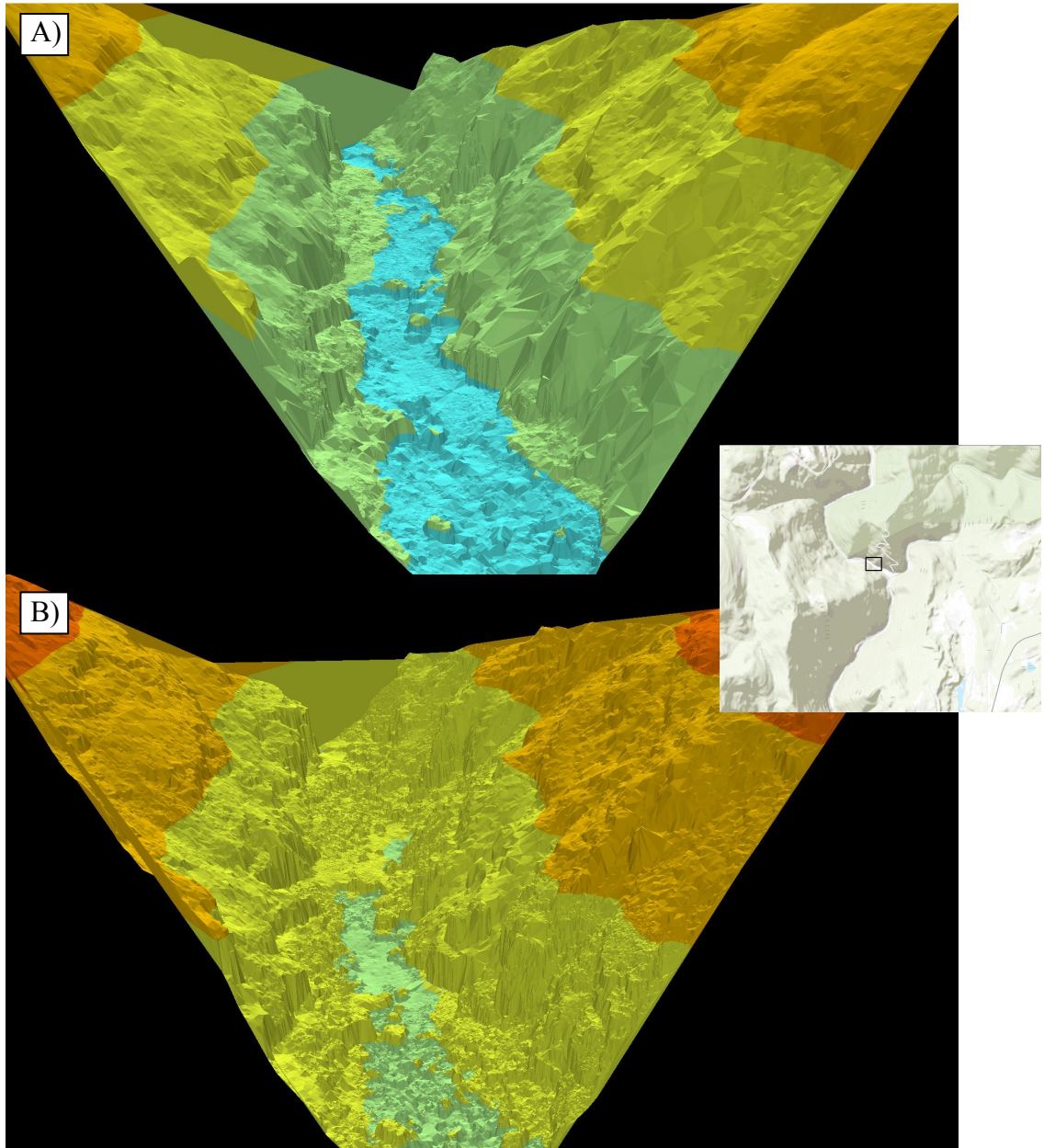


Figure 9. Oblique view example of pre (A) and post (B) LiDAR re-filtering.

5. Supplemental Data

Several deep pools are present within the study area river corridor with depths preliminary estimated to exceed 20 feet. Despite the excellent LiDAR penetration, the survey did not yield ground returns for numerous in-water areas throughout the river corridor (Fig. Error! Reference source not found.). Conservatively, no data was obtained for approximately 10.1 acres or 22.06% of in-water areas of the river corridor. Limited access and rugged terrain within the river canyon prevent kayak and foot access to much of these areas. In order to fill in these data gaps, an increasing validated approach linking depth to multi-spectral imagery color ratios was used.

5.1. *Imagery Derived Depth Data*

This method uses the approach developed by Legleiter et al. (2004) and expanded in Legleiter et al. (2009) where water depth is compared to the natural logarithm of different pairs of imagery wavelengths. A simple algorithm, optimal band ratio analysis (OBRA), is used to evaluate different pairs of wavelengths to identify the strongest linear relationships between an image-derived quantity X (the natural logarithm of two wavelengths) and water depth.

For this analysis in order to avoid generating multiple relationships for separate imagery tiles the compressed county mosaic (CCM) 2014 NAIP imagery was used for source imagery. This data includes three spectral band; green (460 nm, width 60 nm); red (635 nm, width 50 nm), and blue (560nm, width 50nm). Imagery was projected from its native WGS 1984 Web Mercator coordinate system into the project coordinate system and georeferenced using the LiDAR intensity data as the reference dataset. Good georeferencing is critical in creating the depth-to-color (depth-to-X) relationship.

A training dataset for the depth-to-X relationship was generated from the re-filtered LiDAR ground points. In order to improve performance of the training set, points were limited to in-water areas with depths greater than 2 feet. Edge effects were minimized by selecting points at least 2 meters from the delineated edge of water. A total of 137,022 points were included in the training set. For each point the underlying band wavelength values were sampled and OBRA was used to create linear and/or polynomial regression models.

To determine the best depth-to-X relationship rasters of each resultant X were created and visualized with existing depth data to infer obvious correlating trends in the data. Consistent with literature (Legleiter et al. 2009) Green/Red models showed a potentially strong relationship. However, the Blue/Red models also displayed an equally if not greater correlated depth trend, less overall variance in the relationship, and higher R^2 values, all of which indicated better fits to the depth data. Using sounding depths as a test data set, comparison was made between predictions from several preliminary Green/Red vs. Blue/Red models. The Blue/Red models consistently yielded lower root means square errors (RMSEs) and slope values closer to 1 (e.g. a 1:1 relationship between predicted depth and sounding depth). Therefore, the Blue/Red depth-to-X relationship was considered the best for further testing and use.

Overall, all relationships between depth and X, even Blue/Red, exhibited very high variability (Fig 10). Historically, the imagery derived bathymetry method has been applied to lowland, shallow; relatively clear flowing, gravel-bottom rivers. Research (Legleiter et al. 2009, Legleiter 2012, and Legleiter 2013) has shown that application of this methodology may be problematic or have accuracy influenced by poor georeferencing or co-registration of imagery to depth data, lack of clear water conditions, presence of poorly reflective or heterogeneous substrates, coarse imagery resolution, and deep water conditions. Furthermore, this methodology has been found to be limited to certain maximum detectable depths often less than 6.56 feet (2 meters).

The portions of the study area requiring depth data are characterized by complex and heterogeneous terrain and substrates, varying water turbidity, and many deep water areas. Therefore, the observed depth-to-X variability is not unexpected. Several regression models were generated using different portions of the training data (i.e. the training data was left whole and was split into an upper river and lower river section demarcated by the confluence of the Middle Yuba), binning the data and fitting relationships with the median value of each bin (a smoothing technique), and using both linear and polynomial regressions in attempt to address the variability

and identify the most suitable model(s). Similar to the testing above, the suite of models was compared to each soundings data set, respectively, to identify potential location specific or an overall best model(s). A similar discretized testing method was employed using the entire in-water LiDAR depth dataset. This data was split up into sections along the river where points were compared to each predictive model to ascertain if a specific model performed better within a particular section of river. The final approach included a suite of depth-to-X predictive models spatially distributed along the river.

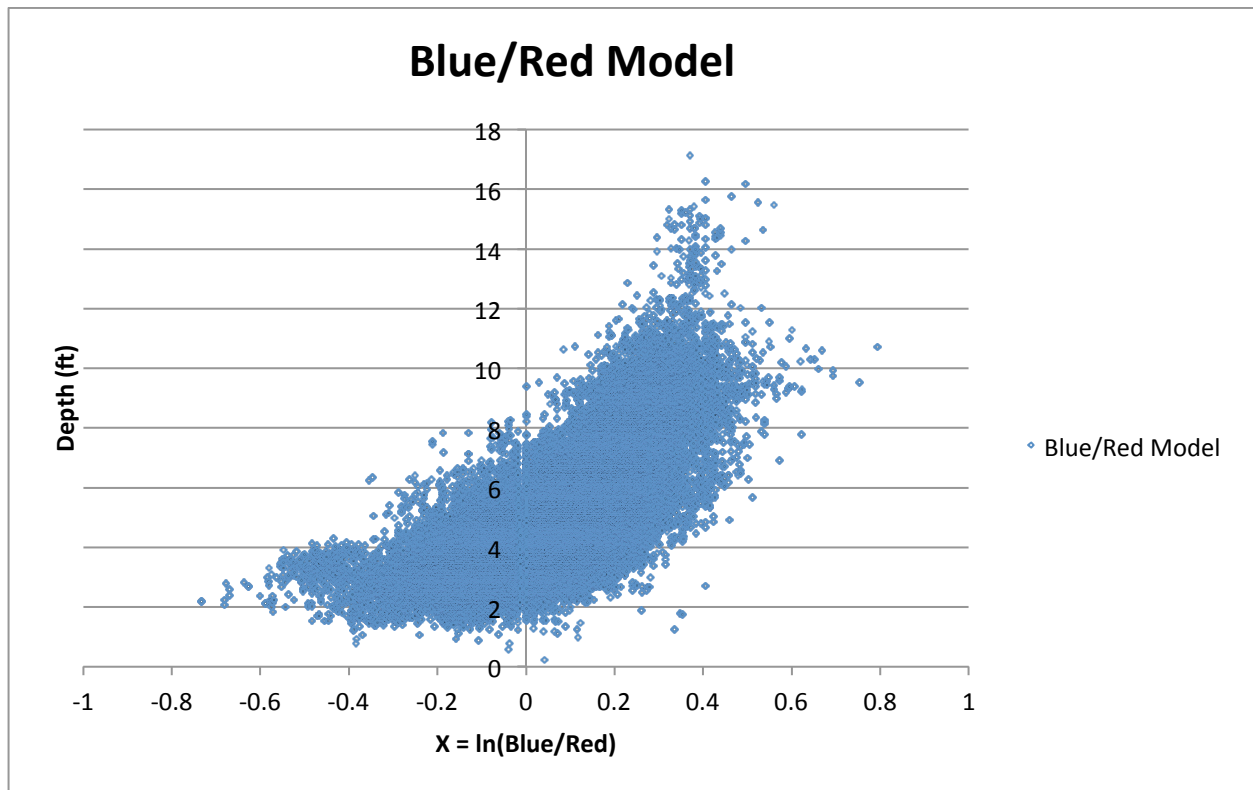


Figure 10. Blue/red depth-to-X scatterplot for all LiDAR training data.

Figure 11 depicts an example of the final depth prediction raster data. Given the potential prediction issues described in this section, the resulting raster data was thoroughly vetted for quality assurance/quality control (QA/QC). Depth rasters were visualized in 3D to identify areas of severe over or under prediction that were subsequently excluded from the final topographic map. Areas of over prediction were common along channel margins and in shadows. The vetted depth prediction raster data was converted to land surface elevations using the WSE data similar to the processed described in Section 3.3.1 and then converted to point data for incorporation into the final ground dataset (Section 6). A total of 168,965 additional ground points covering an area of ~3.9 acres were derived from this method and included in the final topographic map.

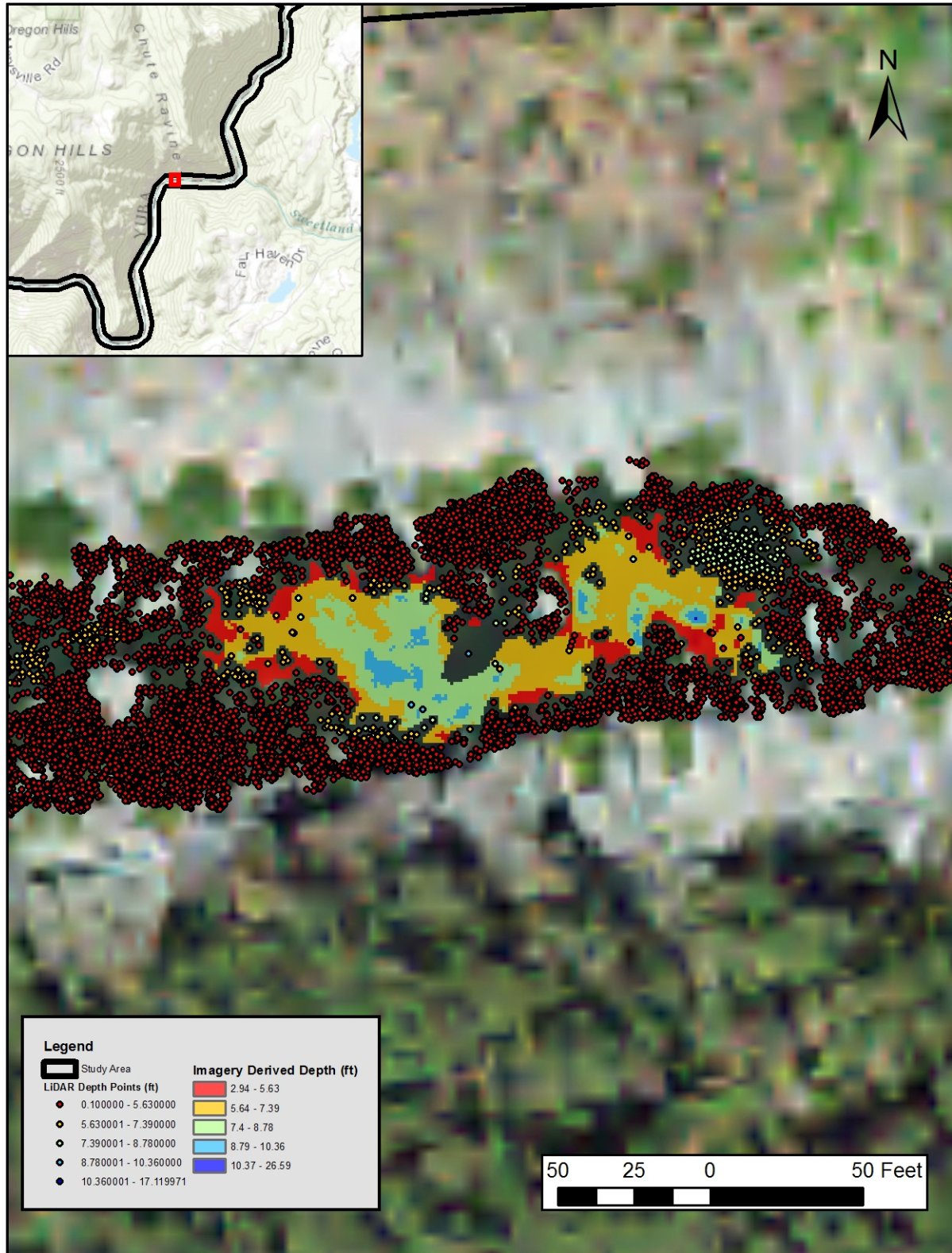


Figure 11. Example of imagery derived bathymetric data.

5.2. *Augmented Points*

The imagery derived depth data discussed in Section 5.1 served to fill a significant portion of the gaps in the topographic map. However several areas where depth prediction remained infeasible or highly inaccurate (e.g. areas in imagery with high surface turbulence or shadows, channel margins, or other edges) continued to lack data. Visualization of a preliminary interpolated topographic map was used to identify remaining areas where interpolation alone was unable to characterize an appropriate ground surface. Using the available LiDAR, soundings, and reliable imagery derived depth data these remaining areas were systematically addressed manually through the addition of strategically placed “augmented points”. Point depths/elevations were assigned manually based on best professional judgement and neighboring points. A total of 828 additional “augmented” ground points were manually input and included in the final topographic map.

6. **Conclusion**

Bathymetric LiDAR delivered tremendously high resolution data with substantial coverage of the study area in just several days’ worth of mapping. Two additional days were spent gathering SB sonar points in several deep pools where data was missing. Analysis of the LiDAR data revealed potential over-filtering of ground returns as well as large areas lacking any data. Cutting edge techniques were used to address these issues with a high level of QA/QC. The final topographic maps consists of the re-filtered LiDAR ground points, SB sonar, imagery derived depth points, and augmented points.

Thorough verification and merging of each individual dataset an extremely detailed and accurate topographic surface of the project area was created. Table 9 provides a summary comparing the initial LiDAR ground data provided by Quantum Spatial to the final dataset. The summary includes information for both the entire extent of the LiDAR acquisition and specific to the study area, which was the focal point of the re-filtering process. These increases in point density provide a high quality topographic map of the study area, allowing for production of improved 2-D hydrodynamic models.

Table 9. Original vs. final topographic data summary.

Dataset	Total Ground Points	Average Point Spacing (ft)	Average Point Density (points/ft ²)	Percent difference # of points from Quantum Spatial ¹	Percent difference point spacing from Quantum Spatial ¹	Percent difference point density from Quantum Spatial ¹
Quantum Spatial ground LiDAR	20901576	1.94	0.27	N/A	N/A	N/A
Final ground surface	69784144	1.09	0.84	233.87%	-43.81%	211.11%
Quantum Spatial ground LiDAR (Study Area)	5388037	1.68	0.35	N/A	N/A	N/A
Final ground surface (Study Area)	21279867	0.82	1.49	294.95%	-51.19%	325.71%

¹Percent differences are relative to the appropriate quantum spatial dataset, i.e. either the entire dataset or the study area, respectively.

7. References

- Axelsson, P. 2000. DEM Generation from Laser Scanner Data Using Adaptive TIN Models. *International Archives of Photogrammetry and Remote Sensing* 34: 110-116.
- Bureau of Reclamation (BOR), 2012. Literature Review Focused on Data Processing Techniques for the Selective Filtering of Light Detection and Ranging (LiDAR) Data for Enhanced Surface Representation of River Geomorphology. Project ID 657. Available online at <http://www.usbr.gov/research/projects/detail.cfm?id=657>
- Carley, J. K., Pasternack, G. B., Wyrick, J. R., Barker, J. R., Bratovich, P. M., Massa, D. A., Reedy, G. D., Johnson, T. R. 2012. Significant decadal channel change 58-67 years post-dam accounting for uncertainty in topographic change detection between contour maps and point cloud models. *Geomorphology* 179: 71-88, doi:10.1016/j.geomorph.2012.08.001.
- ESRI. 2012. Image classification using the ArcGIS Spatial Analyst extension. Available online at: <http://resources.arcgis.com/EN/HELP/MAIN/10.1/index.html#//00nv00000003000000>
- Gilbert, G. K. 1917. Hydraulic-mining debris in the Sierra Nevada. in D. o. t. Interior, editor. United States Geological Survey, Washington, D.C.
- Legleiter, C. J. 2012. Remote measurement of river morphology via fusion of LiDAR topography and spectrally based bathymetry, *Earth Surface Processes and Landforms* 37: 499–518.
- Legleiter, C. J. 2013. Mapping river depth from publicly available aerial images, *River Res. Appl.*, 29(6), 760–780.
- Legleiter, C. J., Roberts, D. A., Marcus, W. A., and Fonstad, M. A., 2004. Passive optical remote sensing of river channel morphology and in-stream habitat: Physical basis and feasibility. *Remote Sensing of Environment* 93-4, 493-510.
- Legleiter CJ, Roberts DA, Lawrence RL. 2009. Spectrally based remote sensing of river bathymetry. *Earth Surface Processes and Landforms* 34: 1039–1059. DOI: 10.1002/esp.1787.
- Pasternack, G.B., 2011. 2D Modeling and Ecohydraulic Analysis. Createspace, Seattle, WA.
- Pasternack, G. B. and Senter, A.E. 2011. 21st Century instream flow assessment framework for mountain streams. California Energy Commission, PIER. CEC-500-2013-059.
- Sithole G. and G. Vosselman. 2004. Experimental comparison of filter algorithms for bare-Earth extraction from airborne laser scanning point clouds. *ISPRS Journal of Photogrammetry and Remote Sensing*, 59:85-101.

Snyder, N. P., D. M. Rubin, C. N. Alpers, J. R. Childs, and J. A. Curtis. 2004. Estimating accumulation rates and physical properties of sediment behind a dam: Enlebright Lake, Yuba River, northern California. USGS Staff - Published Research Paper 489.

Yuba County Water Agency (YCWA). 2012. Yuba River Development Project FERC Project No. 2246. Model Report Appendix A. Hydrology Report. June 2012.

Zhang, K. and D. Whitman. 2005. Comparison of three algorithms for filtering airborne LIDAR data. *Photogrammetric Engineering & Remote Sensing*, 71(3):313-324.